Lab on a Chip

RSCPublishing

Home Publishing Journals Lab on a Chip Advance Articles DOI: 10.1039/c004521g

Lab Chip, 2010 | DOI: 10.1039/c004521g | Paper

Digital PCR on a SlipChip†

Feng Shen , Wenbin Du , Jason E. Kreutz , Alice Fok and Rustem F. Ismagilov *
Department of Chemistry and Institute for Biophysical Dynamics, The University of Chicago, 929 E 57th St, Chicago, Illinois 60637, USA. E-mail: r-ismagilov@uchicago.edu

Received 22nd March 2010 , Accepted 9th June 2010

First published on the web 1st July 2010

This paper describes a SlipChip to perform digital PCR in a very simple and inexpensive format. The fluidic path for introducing the sample combined with the PCR mixture was formed using elongated wells in the two plates of the SlipChip designed to overlap during sample loading. This fluidic path was broken up by simple slipping of the two plates that removed the overlap among wells and brought each well in contact with a reservoir preloaded with oil to generate 1280 reaction compartments (2.6 nL each) simultaneously. After thermal cycling, end-point fluorescence intensity was used to detect the presence of nucleic acid. Digital PCR on the SlipChip was tested quantitatively by using *Staphylococcus aureus* genomic DNA. As the concentration of the template DNA in the reaction mixture was diluted, the fraction of positive wells decreased as expected from the statistical analysis. No cross-contamination was observed during the experiments. At the extremes of the dynamic range of digital PCR the standard confidence interval determined using a normal approximation of the binomial distribution is not satisfactory. Therefore, statistical analysis based on the score method was used to establish these confidence intervals. The SlipChip provides a simple strategy to count nucleic acids by using PCR. It may find applications in research applications such as single cell analysis, prenatal diagnostics, and point-of-care diagnostics. SlipChip would become valuable for diagnostics, including applications in resource-limited areas after integration with isothermal nucleic acid amplification technologies and visual readout.

Introduction

This paper describes a simple SlipChip-based method for counting nucleic acid molecules *via* digital PCR. Digital PCR[1–9] is a powerful method to detect rare cells and count cells, DNA, and RNA, and relies on the single-molecule sensitivity of PCR. At the single molecule level, confining the molecule in a small volume increases the relative concentration, thus increasing the sensitivity.[10] In digital PCR, after a statistical analysis, the number of "positive" wells approximately corresponds to the number of target molecules in the sample.

Digital PCR has been previously demonstrated on a multiwell plate,[1,5] and in a number of microfluidic formats.[2,6,11–13] Valve-controlled microfluidic chips have adapted digital PCR for various applications, such as cell analysis[2,4] and prenatal diagnosis;[6,14] however, this method still requires a complex fabrication process and a pneumatic system to control the opening and closing of the valves. Another system for digital PCR uses picolitre droplets in a microfluidic device for single-copy PCR and RT-PCR.[11,12] Droplet-based approaches are attractive for a wide range of applications,[15,16] but they require pumping equipment and equipment for rapid readout. A spinning disk platform was also recently developed for digital PCR,[13] but it still requires centrifugation for fluid control. Emulsion PCR,[17] microdroplet,[18] and engineered nanolitre droplets[19] can be also potentially applied for digital PCR, but these systems require either mechanical agitation or pumps to generate the small volume droplets. A microfluidic chamber for high throughput nanolitre volume quantitative PCR[20] can also be adapted for digital PCR, but it still requires mechanical loading and manual sealing operations.

A simple, inexpensive platform is still an unmet need to make digital PCR a routine procedure in laboratories or resource-limited settings. In this paper, we describe such a system based on the SlipChip platform.[21–26] The SlipChip relies on movement, or "slipping", of two plates imprinted with wells and ducts to convert continuous fluidic paths

used for filling a device into discreet volumes suitable for compartmentalization of nucleic molecules required for digital PCR. Therefore, it can achieve compartmentalization without requiring a complex fabrication process or a complex manipulation system. As the plates are slipped past one another, the wells and ducts are brought in and out of contact to combine reagents and perform reactions. The SlipChip platform has been shown to handle multistep processes on many small volumes in the context of protein crystallization[21–23] and immunoassays.[25] In parallel studies, multiplexed PCR was successfully demonstrated in the SlipChip:[26] no cross-contamination was seen when different preloaded primers were used to screen a sample to identify the presence of pathogens, and the design of the SlipChip was modified to allow room for thermal expansion of the aqueous PCR solution during thermal cycling. Here, we test and quantify the performance of SlipChip using single-molecule amplification in digital PCR.

Experimental section

Chemicals and materials

All solvents and salts purchased from commercial sources were used as received unless otherwise stated. SsoFast EvaGreen Supermix (2X) was purchased from Bio-Rad Laboratories (Hercules, CA). Bovine serum albumin (BSA) was purchased from Roche Diagnostics (Indianapolis, IN). All primers were ordered from Integrated DNA Technologies (Coralville, IA). Mineral oil (DNase, RNase, and Protease free) and DEPC-treated nuclease-free water were purchased from Fisher Scientific (Hanover Park, IL). Dichlorodimethylsilane was purchased from Sigma-Aldrich (St Louis, MO). *Staphylococcus aureus* genomic DNA (ATCC number 6538D-5) was purchased from American Type Culture Collection (Manassas, VA). PCR tubes and barrier pipette tips were purchased from Molecular BioProducts (San Diego, CA). Mastercycler and *in situ* adapter were purchased from Eppendorf (Hamburg, Germany). Spectrum food colors (red food dye) were purchased from August Thomsen Corp (Glen Cove, NY). Soda-lime glass plates coated with chromium and photoresist were purchased from Telic Company (Valencia, CA). Photomasks were obtained from CAD/Art Services, Inc. (Bandon, OR). Amorphous diamond coated drill bits were obtained from Harvey Tool (0.030 inch cutter diameter, Rowley, MA).

Fabrication of SlipChip for digital PCR

The procedure for fabricating the SlipChip was based on the procedure described in previous work.[21] The soda-lime glass plate coated with chromium and photoresist was aligned with a photomask containing the design for the wells (both circular and elongated) of the SlipChip, and AZ 1500 positive photoresist was exposed using standard exposure protocols. Immediately after exposure, the glass plate was immersed in 0.1 mol L^{-1} NaOH to remove the areas of the photoresist exposed to UV light. The exposed underlying chromium layer was removed using a chromium etchant (a solution of 0.6 : 0.365 mol L^{-1} $HClO_4/(NH_4)_2Ce(NO_3)_6$). The glass plate was then rinsed with Millipore water and dried with nitrogen gas. The back of the glass plate was taped with PVC sealing tape to protect the glass, and the taped glass plate was then immersed in a glass etching solution (1 : 0.5 : 0.75 mol L^{-1} $HF/NH_4F/HNO_3$) to etch the glass surface where chromium coating was removed in the previous step. Etching speed was controlled by controlling the temperature, and 35 min etching time at 40 °C produced wells that were 50 μm deep.

The glass plate with an etched pattern of wells was thoroughly cleaned with reverse-osmosis purified (Millipore) water and ethanol and dried with nitrogen gas. The glass plate was oxidized in a plasma cleaner for 100 seconds and immediately placed in a desiccator with 50 μL of dichlorodimethylsilane. A vacuum was then applied for one hour for gas-phase silanization. The silanized glass plate was rinsed with chloroform, acetone, and ethanol, and then dried with nitrogen gas. In order to be reused, the glass plate could be cleaned with piranha acid (3 : 1 sulfuric acid : hydrogen peroxide) and silanized again as described above.

Assembling and loading the SlipChip

The mineral oil was filtered and degassed before using. The SlipChip was assembled under mineral oil. The bottom plate was first immersed into the oil in a Petri dish, with the patterned side facing up. The top plate was then laid on top of the bottom plate with the patterned side facing down. The two plates were assembled as shown in Fig. 1d–f under the stereomicroscope for precise alignment, and then the aligned SlipChip was fixed using binder clips.

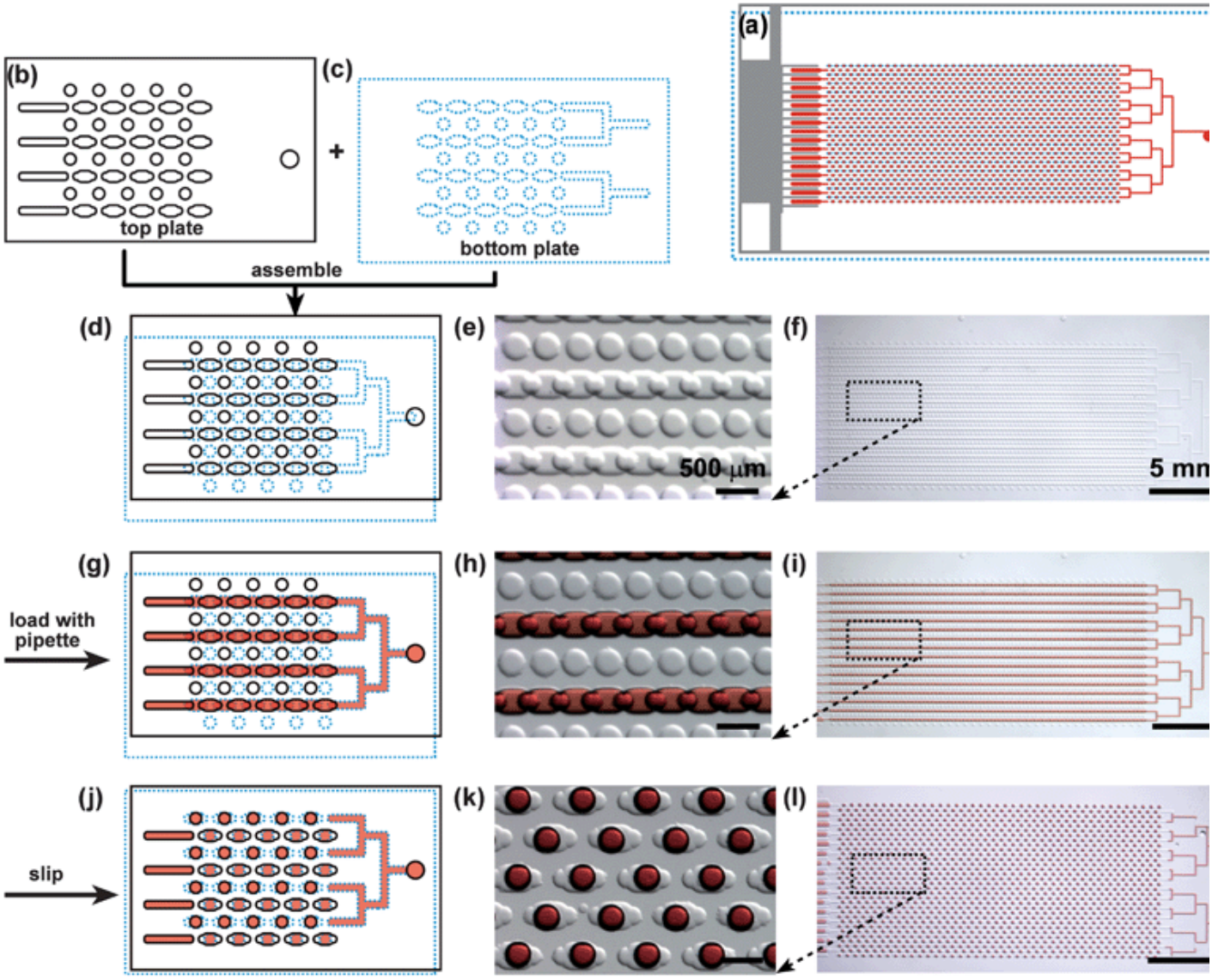

Fig. 1 Schematic drawing and bright field images show the design and mechanism of the SlipChip for digital PCR. The top plate is outlined with a black solid line, the bottom plate is outlined with a blue dotted line, and red represents the sample. (a) Schematic drawing shows the design of the entire assembled SlipChip for digital PCR after slipping. (b) Schematic drawing of part of the top plate. (c) Schematic drawing of part of the bottom plate. (d–f) The SlipChip was assembled such that the elongated wells in the top and bottom plates overlapped to form a continuous fluidic path. (g–i) The aqueous reagent (red) was injected into SlipChip and filled the chip through the connected elongated wells. (j–l) The bottom plate was slipped relative to the top plate such that the fluidic path was broken up and the circular wells were overlaid with the elongated wells, and aqueous droplets were formed in each compartment. (d, g and j) Schematic of the SlipChip; (e, h and k) zoomed in microphotograph of the SlipChip; (f, i and l) microphotograph of the entire SlipChip.

Aqueous solution was loaded into the SlipChip by pipetting into the inlet. A dead-end filling method[27] was applied to fill all the wells evenly, so that there was no outlet for aqueous solution. As the aqueous solution flowed in, the

mineral oil present in the wells was expelled through the gap between the glass plates. To avoid accidental injection of air bubbles into the chip, 6 μL of aqueous solution were used for injection until the entire fluidic path was filled with aqueous solution.

PCR amplification

Primer sequences for the *nuc* gene found in *S. aureus* were selected from a previous publication:[28] 5′-GCGATTGATGGTGATACGGTT-3′ (primer 1) and 5′-AGCCAAGCCTTGACGAACTAAAGC-3′ (primer 2). The reaction master mixture consisted of 10 μL of 2X SsoFast EvaGreen Supermix, 0.5 μL of primer 1 (10 μmol L^{-1}), 0.5 μL of primer 2 (10 μmol L^{-1}), 2 μL of 10 mg mL^{-1} BSA solution, 5 μL of nuclease-free water and 2 μL of *S. aureus* genomic DNA (gDNA) solution. The *S. aureus* gDNA solution was serially diluted using 1× BSA solution (0.01 mg mL^{-1}), and the range of final template concentrations in the PCR mixture was: 1 ng μL^{-1}, 100 pg μL^{-1}, 10 pg μL^{-1}, 1 pg μL^{-1}, 100 fg μL^{-1}, 10 fg μL^{-1}, and 1 fg μL^{-1}. The concentration of DNA stock solution was measured spectrophotometrically by NanoDrop (Thermo scientific). The amplification was performed using a PCR thermocycling machine (Eppendorf). To amplify the DNA, an initialization step of 2 min at 94 °C was used to activate the enzyme. Next, a total 35 cycles of amplification were performed as follows: a DNA denaturation step of 1 min at 94 °C, a primer annealing step of 30 s at 55 °C, and a DNA extension step of 30 s at 72 °C. After the final cycle, a final elongation step was performed for 5 min at 72 °C. Then the PCR products were stored in the cycler at 4 °C before imaging.

DNA copy number calculation

We estimated 1 ng of *S. aureus* gDNA contains approximately 3×10^5 copies. The volume of reaction solution in each compartment was 2.6 nL, and at the gDNA concentration of 1 ng μL^{-1}, the copy number of gDNA per well was expected to be approximately 8×10^2 copies per well.

Image acquisition and analysis

Bright field images were acquired with a Leica stereomicroscope. All fluorescence images were acquired by using a digital camera (C4742, Hamamatsu Photonics, Japan) mounted to a Leica DMI 6000 B epi-fluorescence microscope with a 5×/0.15 NA objective and L5 filter at room temperature. All fluorescence images were corrected by a background image obtained with a standard fluorescent slide and then stitched together using MetaMorph software (Molecular Devices, Sunnyvale, CA). Each image in Fig. 3 was automatically stitched together by using forty fluorescence images. The intensity levels were adjusted to the same values for all images.

Measuring size variation of droplets formed in the SlipChip

The PCR mastermix was injected into the assembled SlipChip as described above. Two-dimensional fluorescent images were taken, and all the images were corrected by using a background image and thresholded to the same value. The number of pixels comprising each droplet, along with the mean and standard deviation for all 1280 droplets, was determined using MetaMorph software. The variation of the two-dimensional cross-section of the droplets formed in the SlipChip was calculated to be approximately 5% across all 1280 wells. This variation could be further decreased by optimizing the geometry of the wells on both the top and bottom plates.

Results and discussion

The design of the device was symmetric to increase the density of wells (Fig. 1a). Arrays of circular wells filled with oil were designed in both the top and bottom plates, and overlapping elongated wells in both top and bottom plates (Fig. 1b–c), were used to introduce the sample (Fig. 1d–i). Upon slipping, isolated compartments were created (Fig. 1j–l), and an aqueous droplet of uniform size was generated in each individual compartment. This SlipChip contained no ducts to load the sample; instead, each plate was patterned with alternating rows of the elongated wells and circular wells for a total 1280 reaction compartments. The elongated wells were 400 μm long, 200 μm wide, and 50 μm deep, and the circular wells were 200 μm in diameter and 50 μm in depth (Fig. 1). In the initial configuration, the elongated wells in the top and bottom plates overlapped to form a continuous fluidic path (Fig. 1d–f). Using overlapping elongated wells instead of wells connected by ducts provided two advantages: (i) no sample was wasted in the ducts and (ii) the pressure drop in the device was reduced, allowing 1280 wells to be filled easily by a single

pipetting step (Fig. 1g–i). By slipping the top plate relative to the bottom plate, the elongated wells were separated and each was centered on top of a circular well containing the lubricating fluid (mineral oil) (Fig. 1j–l). For digital PCR, the primer was added to the PCR mixture instead of being preloaded into the circular wells as previously described.[26] The elongated wells were designed so that the width of the elongated wells was the same as the diameter of the circular wells. This design had three advantages: (1) it enabled the resulting aqueous droplets to be centered in the wells, allowing for better imaging. (2) It also produced droplets of consistent volume (~2.6 nL). (3) It created an aqueous droplet surrounded by oil within the well, as in the multiplexed PCR SlipChip,[26] eliminating potential problems associated with thermal expansion during thermal cycling.

During thermal cycling, the lubricating fluid and the aqueous PCR mixture expand more than the glass material of the SlipChip due to the different thermal expansion coefficients of the three materials, potentially leading to cross-contamination due to leakage of the aqueous solution into the gap between the two plates. In the multiplexed PCR SlipChip, we solved this problem by overlapping a square well containing an aqueous PCR mixture with a circular well containing oil, producing a droplet suspended in oil and centered in the square well.[26] For digital PCR, we achieved the same result by using elongated wells containing the aqueous PCR mixture centered over circular wells filled with the lubricating fluid.

We first tested digital PCR on the SlipChip with 10 fg μL^{-1} of *S. aureus* gDNA. At this concentration, there was less than 1 copy of gDNA per 100 wells on average, and PCR amplification of single copy of gDNA was achieved. A linescan of the digital PCR SlipChip before and after thermal cycling (Fig. 2) shows that the fluorescence intensity for wells containing a single DNA template increased significantly while the fluorescence intensity for wells without DNA template did not increase. This linescan also verified that there was no cross-contamination in the SlipChip, as the fluorescence intensity for negative wells adjacent to a well containing DNA template did not change.

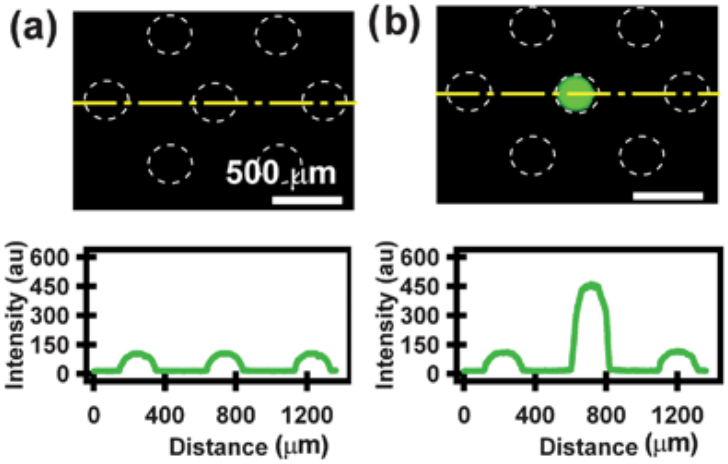

Fig. 2 Amplification of single copy of gDNA by using digital PCR on the SlipChip. (a) Fluorescence microphotograph shows part of the SlipChip before thermal cycling, and the linescan presents the fluorescence intensity along the yellow dashed line. The white dashed line outlines the edge of droplets formed in the wells. (b) Fluorescence microphotograph acquired at the same position after thermal cycling: only the center well shows a significant increase in fluorescence from background. The linescan presents the fluorescence intensity along the yellow dashed line.

We quantified the performance of this device using five concentrations of genomic DNA from *S. aureus* (Fig. 3). The digital PCR SlipChip was able to detect template DNA at concentrations as low as 1 fg μL^{-1}. The expected concentration of the DNA template was presented as number of copies per well (cpw), and the concentration of the original DNA stock solution was measured spectrophotometrically. The detailed method for calculating the cpw is presented in the Experimental section. As the DNA template in the PCR master mixture was diluted, the fraction of positive wells decreased proportionally (Fig. 3a–e and 4). We saw no evidence of contamination, as a control sample containing no template DNA did not give any positive results (Fig. 3f).

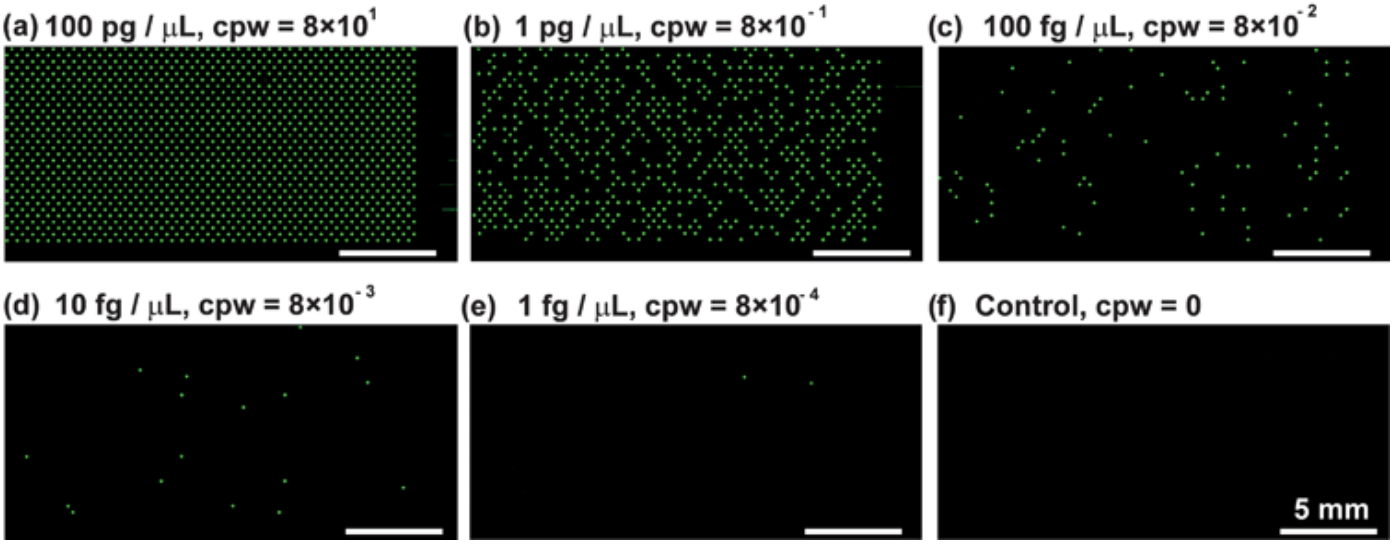

Fig. 3 Digital PCR on the SlipChip with different concentrations of *S. aureus* gDNA. (a–e) Digital PCR on the Slipchip with a serial dilution of target DNA template ranging from 100 pg μL^{-1} to 1 fg μL^{-1}. Concentrations of gDNA and expected copies per well (cpw) are indicated above each figure. (f) Control, no wells showed positive signal when no target DNA template was loaded.

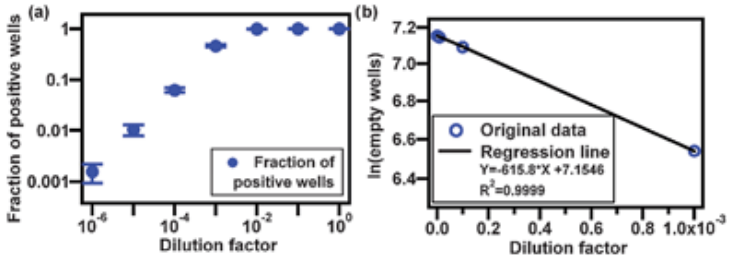

Fig. 4 Quantified results of digital PCR experiments. (a) Experimental average fraction of positive wells as a function of dilution factor from an initial concentration of 1 ng of *S. aureus* gDNA per μL. Error bars represent standard deviation of the experiment ($n \geq 3$ for the experimental measurement of fraction of positive wells). (b) Regression fit of results from the four most diluted samples (lowest dilution factors).

We repeated the experiments for each concentration ($n \geq 3$), and generated a curve relating the fraction of positive wells to the dilution factor (Fig. 4a). The dilution factor was calculated from the initial concentration of 1 ng μL^{-1}. A regression fit of eqn (1) (linearized form of the Poisson equation) was used to characterize the performance of the device. In eqn (1), f is the number of positive wells, c is the initial concentration of the sample prior to dilution (in genome copies per well), x is the fractional dilution factor of the original concentration (in units of concentration^{-1}, where 10 fold dilution corresponds to $x = 0.1$), and n is the total number of wells. $n - f = s$, where s is the number of negative wells. (See ESI† for derivation.)

$$\ln(n - f) = -c \times x + \ln n \quad (1)$$

Constraining the intercept to equal ln 1280 when plotting x *vs.* $\ln(n - f)$ will give a slope equal to the negative of the original concentration (Fig. 4b). Fitting the equation without constraining the intercept gives a comparable result,

supporting the appropriate use of the fit as a method of estimation. The excellent fit obtained (Fig. 4b) indicates that the device produces self-consistent results that follow Poisson statistics.

We note that the method of eqn (1), while suitable for testing the performance of the device, is not always correct for extracting the starting concentration of the undiluted sample. Under non-ideal conditions, where different dilutions may give inconsistent results, this method does not weigh all observed results equally. Most probable number (MPN) theory, which maximizes the probability of the combined binomials for the different dilutions,[29] is more appropriate for analysis of dilution series that lead to non-ideal results. Results obtained in this paper were sufficiently self-consistent that both methods produced equivalent results. Using data for the four most diluted samples, eqn (1) gives original concentration c of 616 genome copies per well and MPN theory gives 625 genome copies per well. Using data for the five most diluted samples, eqn (1) gives original concentration c of 505 genome copies per well and MPN theory gives 597 genome copies per well. MPN calculations are more laborious; therefore, when the results at multiple dilutions are self-consistent, eqn (1) provides a good approximation.

The estimated original concentration from the fit (Fig. 4b, slope of regression line), ~6.2×10^2 genome copies per well, was within a factor of 1.3 of the concentration determined by spectrophotometry (8×10^2 genome copies per well, see Experimental section, "DNA copy number calculation"). We consider this level of agreement satisfactory because there is some uncertainty associated with the concentration determined by spectrophotometry. Because the exact length of the genome for this strain is unknown and there is uncertainty in the absorption coefficient used, the measured 8×10^2 genome copies per well is an approximation. In addition, potential pipetting error during dilution and potential losses of DNA during sample preparation could increase the deviation between the two estimates.

Next, we performed a more detailed analysis to establish the confidence intervals to interpret each digital measurement. We had two goals: first, we wished to check that there were no significant spatial biases in the performance of the device. For example, losses of DNA on the surface of the device during filling could lower the actual concentration of DNA towards the "outlet" side of the device, leading to lower frequency of positive wells on that side of the device. Second, we wished to establish the reliability of the measurements at the extremes of the dynamic range of this chip, both at low concentrations resulting in only a few positive wells or at high concentration resulting in only a few negative wells. Confidence intervals (CIs) using a normal approximation of the distribution, which is binomial with the probability derived from the Poisson equation, are given by eqn (2),[30–34] sometimes referred to as the Wald method, where p is the probability that a well is negative, n is the total number of wells, and α is the coefficient that sets the confidence interval.

$$\mathrm{CI} = p \pm \alpha \times \sqrt{\left(p \times (1-p)\right)/n} \qquad (2)$$

For the 95% CI, α is 1.96. If the starting concentration is known, p can be calculated using the Poisson equation, which simplifies to $p = e^{-\lambda}$ to determine the probability that a well is negative, where λ is the average concentration per well. The probability that a well contains at least one particle and so gives a positive result is then $1 - p$. Alternatively, if the concentration is unknown, the number of negative wells can be used to estimate the probability using $p = s/n$. This simple approach for calculating CIs is applicable when many compartments (>50 is a common cutoff) are available and when concentrations can be controlled to avoid extreme results (very low or very high fraction of positive wells).

It is well known[30,33] but not always appreciated that eqn (2) cannot be used to evaluate confidence intervals if n is not sufficiently large or if p is close to 0 or 1, as the normal approximation is not acceptable under these conditions. For example, blind use of the Wald method to interpret results with up to 3 negative wells out of 1280 gives a lower limit on p that is negative. Additionally, in the range where the criteria for suitability are not met, the Wald method gives intervals that are too small, so the nominal 95% CI has an actual coverage of less than 95%. The range of p where this approach is acceptable is dependent on n, so a definitive cutoff for either variable is not possible, and there is a variety of criteria available to determine when using the Wald method is valid.[33] To calculate CIs, numerous more universally applicable methods exist.[30,34–39] Here, we chose to use the "score" or "Wilson" method[30,33,35,37,39] given in eqn (3), which derived in a similar fashion to the Wald method but is based on a different set of criteria.[33,39]

$$\frac{p+\frac{\alpha^2}{2\times n}\pm\alpha\times\sqrt{\left(p\times(1-p)+\frac{\alpha^2}{4\times n}\right)/n}}{\left(1+\frac{\alpha^2}{n}\right)} \quad (3)$$

The score method never gives nonsensical ranges, its average coverage is 95%, and it closely fluctuates around the value over a much greater portion of the range than the Wald method. It is more appealing than "exact" methods[35–38,40] that must be solved iteratively, because the equation can still be rapidly used.

We applied the score method to analyze spatial uniformity of the signal from the devices. We separated each device into four quadrants, and determined whether or not the value of the quadrant fell within the 95% CI of the average value. For the four lowest concentrations presented in Fig. 4b, 50 out of 52 quadrants (96%) fell within the 95% CI, supporting the observation that no positional biases were occurring due to filling effects (Table S1, ESI†).

We also applied the score method to calculate the original concentration, including confidence intervals from the raw data (Fig. 5). Our calculations show that, over the majority of the range of wells, the calculated concentrations for individual experiments give comparable values to one another. Our calculations indicate a dynamic range spanning nearly three orders of magnitude (the bracket in Fig. 5). For example, the range from about 5 negative to 5 positive wells corresponds to the range of concentrations of about 1.5×10^3 DNA molecules mL^{-1} to 2.1×10^6 DNA molecules mL^{-1}. The two highest concentrations underestimate the actual concentration as they saturated the system and were expected to have all positive wells. This indicates that a small percentage of false negatives is present in this system (*e.g.* the defect in Fig. 3a), and that if less than 5 wells are negative the sample should be retested at a diluted concentration. Comparing the estimated concentrations from two separate experiments would reveal whether the first result represented correct concentration or was due to wells with false negative signals.

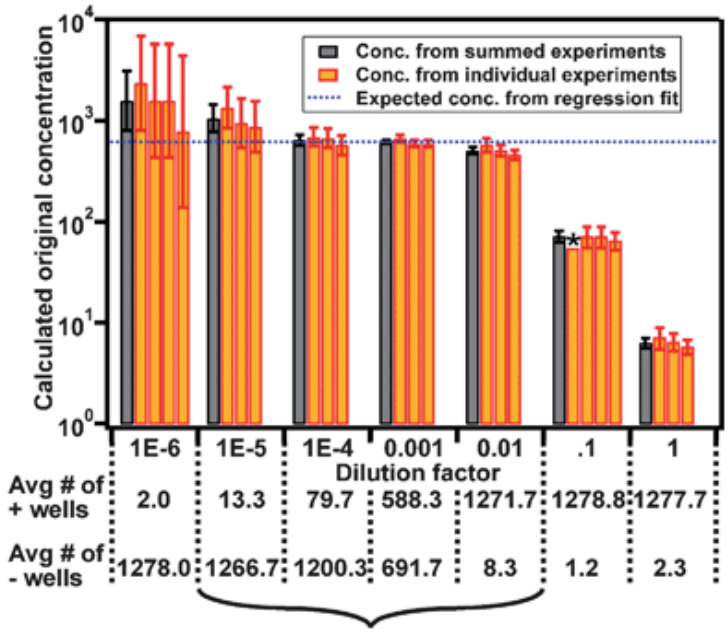

Fig. 5 Analysis of experimental digital PCR data and of confidence intervals predicted by eqn (3). The expected concentration is shown by the blue dashed line, error bars represent the 95% confidence interval. High concentrations saturate the system resulting in incorrect, too-low measurements. The rest of the range gives a more accurate measurement, particularly the range indicated by the bracket. *This experiment resulted in 1280 positive wells so only a lower limit can be determined.

Conclusions

Here we found that the SlipChip was capable of accurately quantifying the amount of nucleic acid present in a sample using standard thermal cycling PCR techniques in a "digital format". The SlipChip contained 1280 wells designed to separate microlitre sample into 1280 droplets of ~2.6 nL each, and was capable of detecting the template DNA at single copy level. The upper limit of concentration that could be detected using this device can be increased by decreasing the individual well volume and/or increasing the number of wells on the SlipChip, and the sensitivity of the device can be improved by increasing the total well volume. We have previously incorporated 16 384 wells of picolitre volume on a single SlipChip with dimensions 1.5 inch by 1 inch (unpublished data). The digital PCR SlipChip would also find additional applications if multiple samples could be screened on the same chip as in SlipChips designed for protein crystallization experiments,[22,23] immunoassays,[25] and multiplex PCR.[26] Multiplex digital PCR SlipChip could be designed to count multiple targets in one experiment without interference by increasing the number of wells and preloading different primer sets in the circular wells. Other improvements to the digital PCR SlipChip design include incorporating isothermal amplification methods such as loop-mediated amplification (LAMP),[41,42] recombinase polymerase amplification (RPA),[43] nucleic acid sequence-based amplification (NASBA),[44–46] transcription-mediated amplification (TMA),[47,48] helicase-dependent amplification,[49,50] rolling-circle amplification (RCA),[51,52] and strand-displacement amplification (SDA),[53,54] and incorporating real-time PCR and multi-color probes, such as the Taqman system and molecular beacons. Multi-color probes can be used to apply digital PCR for multigene detection within a single cell to study heterogeneity and also to provide a method to integrate internal positive controls. Sample preparation such as nucleic acid (DNA/RNA) extraction and purification integrated with the SlipChip would further increase the applicability of this approach.

The SlipChip platform should make digital PCR widely available, and provide a simple quantification of nucleic acids for a wide range of applications. These applications will range from quantification of nucleic acids in research, *e.g.* as is done prior to sequencing,[55] to diagnostic applications, *e.g.* in prenatal diagnostics.[5,56] The device could also be used for single cell analysis such as detection of mutations,[57] monitoring of gene expression,[58] and analysis of cellular heterogeneity.[3,59,60] Another application of digital PCR on the SlipChip is the detection and quantification of rare cells in the presence of normal cells, by distinguishing between mutant and wild-type template DNA or RNA without cross-interference. The SlipChip has the potential to meet the requirements for an ideal diagnostic test in the developing world: affordable, sensitive, specific, user-friendly, rapid, equipment-free, and delivered to those who need it.[61] The current digital PCR SlipChip still requires purified nucleic acid, thermal cycling, and fluorescent readout. As non-thermal cycling methods, nucleic acid purification methods, and simple readouts are incorporated with the digital PCR SlipChip, it could become an analytical and diagnostic tool that is widely available, especially in resource-limited settings.

Acknowledgements

This work was supported by ONR grant No. N00014-08-1-0936, the Camille Dreyfus Teacher-Scholar Awards program, the Chicago Center for Systems Biology (funded by the National Institute of General Medical Sciences at the NIH), and by the NIH Director's Pioneer Award program, part of the NIH Roadmap for Medical Research (1 DP1 OD003584). Part of this work was performed at the Materials Research Science and Engineering Centers microfluidics facility (funded by the National Science Foundation). We thank Elena M. Lucchetta for additional experimental validation and Elena K. Davydova for helpful suggestions in experimental design. We thank Heidi Park for contributions to writing and editing this manuscript.

References

1 B. Vogelstein and K. W. Kinzler, *Proc. Natl. Acad. Sci. U. S. A.*, 1999, **96**, 9236–9241 [Links].

2 E. A. Ottesen, J. W. Hong, S. R. Quake and J. R. Leadbetter, *Science*, 2006, **314**, 1464–1467 [Links].

3 L. Warren, D. Bryder, I. L. Weissman and S. R. Quake, *Proc. Natl. Acad. Sci. U. S. A.*, 2006, **103**, 17807–17812 [Links].

4 J. S. Marcus, W. F. Anderson and S. R. Quake, *Anal. Chem.*, 2006, **78**, 3084–3089 [Links].

5 Y. M. D. Lo, F. M. F. Lun, K. C. A. Chan, N. B. Y. Tsui, K. C. Chong, T. K. Lau, T. Y. Leung, B. C. Y. Zee, C. R. Cantor and R. W. K. Chiu, *Proc. Natl. Acad. Sci. U. S. A.*, 2007, **104**, 13116–13121 [Links].

6 F. M. F. Lun, R. W. K. Chiu, K. C. A. Chan, T. Y. Leung, T. K. Lau and Y. M. D. Lo, *Clin. Chem. (Washington, D. C.)*, 2008, **54**, 1664–1672 [Links].

7 R. A. White, P. C. Blainey, H. C. Fan and S. R. Quake, *BMC Genomics*, 2009, **10**, 116 [Links].

8 T. K. F. Yung, K. C. A. Chan, T. S. K. Mok, J. Tong, K. F. To and Y. M. D. Lo, *Clin. Cancer Res.*, 2009, **15**, 2076–2084 [Links].

9 L. Mazutis, A. F. Araghi, O. J. Miller, J. C. Baret, L. Frenz, A. Janoshazi, V. Taly, B. J. Miller, J. B. Hutchison, D. Link, A. D. Griffiths and M. Ryckelynck, *Anal. Chem.*, 2009, **81**, 4813–4821 [Links].

10 M. E. Vincent, W. Liu, E. B. Haney and R. F. Ismagilov, *Chem. Soc. Rev.*, 2010, **39**, 974–984 [Links].

11 N. R. Beer, B. J. Hindson, E. K. Wheeler, S. B. Hall, K. A. Rose, I. M. Kennedy and B. W. Colston, *Anal. Chem.*, 2007, **79**, 8471–8475 [Links].

12 N. R. Beer, E. K. Wheeler, L. Lee-Houghton, N. Watkins, S. Nasarabadi, N. Hebert, P. Leung, D. W. Arnold, C. G. Bailey and B. W. Colston, *Anal. Chem.*, 2008, **80**, 1854–1858 [Links].

13 S. O. Sundberg, C. T. Wittwer, C. Gao and B. K. Gale, *Anal. Chem.*, 2010, **82**, 1546–1550 [Links].

14 H. C. Fan and S. R. Quake, *Anal. Chem.*, 2007, **79**, 7576–7579 [Links].

15 H. Song, J. D. Tice and R. F. Ismagilov, *Angew. Chem., Int. Ed.*, 2003, **42**, 768–772 [Links].

16 H. Song, D. L. Chen and R. F. Ismagilov, *Angew. Chem., Int. Ed.*, 2006, **45**, 7336–7356 [Links].

17 D. Dressman, H. Yan, G. Traverso, K. W. Kinzler and B. Vogelstein, *Proc. Natl. Acad. Sci. U. S. A.*, 2003, **100**, 8817–8822 [Links].

18 R. Tewhey, J. B. Warner, M. Nakano, B. Libby, M. Medkova, P. H. David, S. K. Kotsopoulos, M. L. Samuels, J. B. Hutchison, J. W. Larson, E. J. Topol, M. P. Weiner, O. Harismendy, J. Olson, D. R. Link and K. A. Frazer, *Nat. Biotechnol.*, 2009, **27**, 1025–1031 [Links].

19 P. Kumaresan, C. J. Yang, S. A. Cronier, R. G. Blazei and R. A. Mathies, *Anal. Chem.*, 2008, **80**, 3522–3529 [Links].

20 R. D. Stedtfeld, S. W. Baushke, D. M. Tourlousse, S. M. Miller, T. M. Stedtfeld, E. Gulari, J. M. Tiedje and S. A. Hashsham, *Appl. Environ. Microbiol.*, 2008, **74**, 3831–3838 [Links].

21 W. B. Du, L. Li, K. P. Nichols and R. F. Ismagilov, *Lab Chip*, 2009, **9**, 2286–2292 [Links].

22 L. Li, W. Du and R. Ismagilov, *J. Am. Chem. Soc.*, 2010, **132**, 106–111 [Links].

23 L. Li, W. Du and R. F. Ismagilov, *J. Am. Chem. Soc.*, 2010, **132**, 112–119 [Links].

24 L. Li and R. F. Ismagilov, *Annu. Rev. Biophys.*, 2010, **39**, 139–158.

25 W. S. Liu, D. L. Chen, W. B. Du, K. P. Nichols and R. F. Ismagilov, *Anal. Chem.*, 2010, **82**, 3276–3282 [Links].

26 F. Shen, W. Du, E. K. Davydova, M. A. Karymov, J. Pandey and R. F. Ismagilov, *Anal. Chem.*, 2010, **82**, 4606–4612 [Links].

27 L. Li, M. A. Karymov, K. P. Nichols and R. F. Ismagilov, *Langmuir*, 2010, DOI:10.1021/la101460z .

28 O. G. Brakstad, K. Aasbakk and J. A. Maeland, *J. Clin. Microbiol.*, 1992, **30**, 1654–1660 [Links].

29 H. O. Halvorson and N. R. Ziegler, *J. Bacteriol.*, 1933, **25**, 101–121 [Links].

30 A. Agresti and B. A. Coull, *Am. Stat.*, 1998, **52**, 119–126 [Links].

31 S. Bhat, J. Herrmann, P. Armishaw, P. Corbisier and K. R. Emslie, *Anal. Bioanal. Chem.*, 2009, **394**, 457–467 [Links].

32 S. Dube, J. Qin and R. Ramakrishnan, *PLoS One*, 2008, **3**, e2876 [Links].

33 L. D. Brown, T. T. Cai, A. DasGupta, A. Agresti, B. A. Coull, G. Casella, C. Corcoran, C. Mehta, M. Ghosh and T. J. Santner, *Stat. Sci.*, 2001, **16**, 101–133.

34 R. G. Newcombe, *Stat. Med.*, 1998, **17**, 857–872 [Links].

35 C. R. Blyth and H. A. Still, *J. Am. Stat. Assoc.*, 1983, **78**, 108–116 [Links].

36 C. J. Clopper and E. S. Pearson, *Biometrika*, 1934, **26**, 404–413 [Links].

37 J. Reiczigel, *Stat. Med.*, 2003, **22**, 611–621 [Links].

38 T. E. Sterne, *Biometrika*, 1954, **41**, 275–278.

39 E. B. Wilson, *J. Am. Stat. Assoc.*, 1927, **22**, 209–212 [Links].

40 M. Li, W. D. Chen, N. Papadopoulos, S. N. Goodman, N. C. Bjerregaard, S. Laurberg, B. Levin, H. Juhl, N. Arber, H. Moinova, K. Durkee, K. Schmidt, Y. P. He, F. Diehl, V. E. Velculescu, S. B. Zhou, L. A. Diaz, K. W. Kinzler, S. D. Markowitz and B. Vogelstein, *Nat. Biotechnol.*, 2009, **27**, 858–863 [Links].

41 T. Notomi, H. Okayama, H. Masubuchi, T. Yonekawa, K. Watanabe, N. Amino and T. Hase, *Nucleic Acids Res.*, 2000, **28**, e63 [Links].

42 E. Aryan, M. Makvandi, A. Farajzadeh, K. Huygen, P. Bifani, S. L. Mousavi, A. Fateh, A. Jelodar, M. M. Gouya and M. Romano, *Microbiol. Res.*, 2010, **165**, 211–220 [Links].

43 O. Piepenburg, C. H. Williams, D. L. Stemple and N. A. Armes, *PLoS Biol.*, 2006, **4**, e204 [Links].

44 J. Compton, *Nature*, 1991, **350**, 91–92 [Links].

45 I. K. Dimov, J. L. Garcia-Cordero, J. O'Grady, C. R. Poulsen, C. Viguier, L. Kent, P. Daly, B. Lincoln, M. Maher, R. O'Kennedy, T. J. Smith, A. J. Ricco and L. P. Lee, *Lab Chip*, 2008, **8**, 2071–2078 [Links].

46 J. W. Romano, K. G. Williams, R. N. Shurtliff, C. Ginocchio and M. Kaplan, *Immunol. Invest.*, 1997, **26**, 15–28.

47 C. Hill, M. Bott, K. Clark and V. Jonas, *Clin. Chem. (Washington, D. C.)*, 1995, **41**, S107–S107.

48 J. Chelliserrykattil, N. C. Nelson, D. Lyakhov, J. Carlson, S. S. Phelps, M. B. Kaminsky, P. Gordon, S. Hashima, T. Ngo, S. Blazie and S. Brentano, *J. Mol. Diagn.*, 2009, **11**, 680–680.

49 Y. J. Jeong, K. Park and D. E. Kim, *Cell. Mol. Life Sci.*, 2009, **66**, 3325–3336 [Links].

50 M. Vincent, Y. Xu and H. M. Kong, *EMBO Rep.*, 2004, **5**, 795–800 [Links].

51 P. M. Lizardi, X. Huang, Z. Zhu, P. Bray-Ward, D. C. Thomas and D. C. Ward, *Nat. Genet.*, 1998, **19**, 225–232 [Links].

52 G. J. Hafner, I. C. Yang, L. C. Wolter, M. R. Stafford and P. M. Giffard, *Biotechniques*, 2001, **30**, 852–857 [Links].

53 G. T. Walker, M. S. Fraiser, J. L. Schram, M. C. Little, J. G. Nadeau and D. P. Malinowski, *Nucleic Acids Res.*, 1992, **20**, 1691–1696 [Links].

54 T. J. Hellyer and J. G. Nadeau, *Expert Rev. Mol. Diagn.*, 2004, **4**, 251–261 [Links].

55 R. A. White, P. C. Blainey, H. C. Fan and S. R. Quake, *BMC Genomics*, 2009, **10**, 116 [Links].

56 H. C. Fan, Y. J. Blumenfeld, Y. Y. El-Sayed, J. Chueh and S. R. Quake, *Am. J. Obstet. Gynecol.*, 2009, **200**, 543 , e541–543, e546.

57 P. S. Bernard and C. T. Wittwer, *Clin. Chem. (Washington, D. C.)*, 2002, **48**, 1178–1185 [Links].

58 J. F. Zhong, Y. Chen, J. S. Marcus, A. Scherer, S. R. Quake, C. R. Taylor and L. P. Weiner, *Lab Chip*, 2008, **8**, 68–74 [Links].

59 U. R. Chandran, C. Q. Ma, R. Dhir, M. Bisceglia, M. Lyons-Weiler, W. J. Liang, G. Michalopoulos, M. Becich and F. A. Monzon, *BMC Cancer*, 2007, **7**, 64 [Links].

60 K. Taniguchi, T. Kajiyama and H. Kambara, *Nat. Methods*, 2009, **6**, 503–506 [Links].

61 M. Urdea, L. A. Penny, S. S. Olmsted, M. Y. Giovanni, P. Kaspar, A. Shepherd, P. Wilson, C. A. Dahl, S. Buchsbaum, G. Moeller and D. C. Hay Burgess, *Nature*, 2006, **444**(suppl. 1), 73–79 [Links].

Footnote

† Electronic supplementary information (ESI) available: derivation of eqn (1), supporting table. See DOI: 10.1039/c004521g